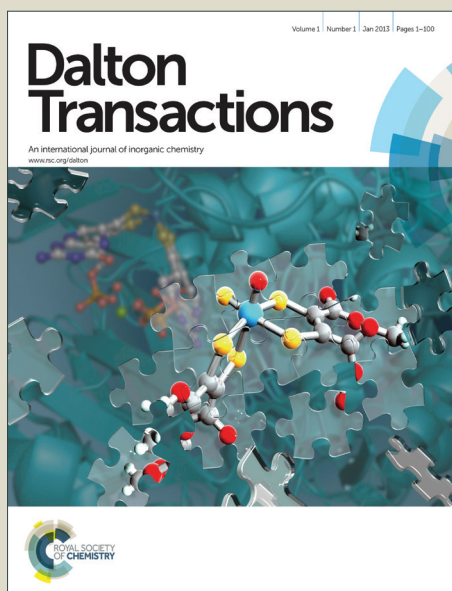


Dalton Transactions

Accepted Manuscript



This article can be cited before page numbers have been issued, to do this please use: D. Das and A. Ghosh, *Dalton Trans.*, 2015, DOI: 10.1039/C5DT01303H.



This is an *Accepted Manuscript*, which has been through the Royal Society of Chemistry peer review process and has been accepted for publication.

Accepted Manuscripts are published online shortly after acceptance, before technical editing, formatting and proof reading. Using this free service, authors can make their results available to the community, in citable form, before we publish the edited article. We will replace this *Accepted Manuscript* with the edited and formatted *Advance Article* as soon as it is available.

You can find more information about *Accepted Manuscripts* in the [Information for Authors](#).

Please note that technical editing may introduce minor changes to the text and/or graphics, which may alter content. The journal's standard [Terms & Conditions](#) and the [Ethical guidelines](#) still apply. In no event shall the Royal Society of Chemistry be held responsible for any errors or omissions in this *Accepted Manuscript* or any consequences arising from the use of any information it contains.

X-ray structurally characterized sensors for ratiometric detection of Zn²⁺ and Al³⁺ in human breast cancer cell (MCF7): Development of binary logic gate as molecular switch

Cite this: DOI: 10.1039/x0xx00000x

Received 00th January 2012,
Accepted 00th January 2012

DOI: 10.1039/x0xx00000x

www.rsc.org/

Abhijit Ghosh and Debasis Das*

Department of Chemistry, The University of Burdwan, Golapbag, Burdwan, India, Fax: +91-342-2530452; Tel: +91-342-2533913 (ext. 424); E-mail: ddas100in@yahoo.com

A very simple molecule derived from salisaldehyde and N-phenyl ethylenediamine (L1) functions as dual-mode ratiometric fluorescence “turn on” sensors for Zn²⁺ and Al³⁺ at two different wavelengths. The sensing is based on the combined effect of inhibition of excited-state intra-molecular proton transfer (ESIPT), CH=N isomerization and chelation-enhanced fluorescence (CHEF). Moreover, [L1+Zn²⁺] system functions as better Al³⁺ sensor where Al³⁺ ratiometrically displaces Zn²⁺ from [L1+Zn²⁺] complex. Emission wavelength dependent differentiation of Zn²⁺ and Al³⁺ using L1 allows us to develop a binary logic gate that functions as a molecular switch. L1 efficiently detects Zn²⁺ and Al³⁺ in human breast cancer cell (MCF7) while [L1+Zn²⁺] complex specifically detects Al³⁺ in the said cells.

Chemosensors that convert molecular recognition event into highly sensitive and easily detectable signals are being actively studied as an attractive research area indeed. The imaging techniques to visualize bio-active metal ions have got superior importance in biomedical analysis and environmental monitoring. Fluorescence technique has emerged as most powerful tool for its operational simplicity, high sensitivity and cost effective methodology.^{1,2}

Particularly, when ratiometric sensor exhibits spectral shift upon interaction with specific analyte, then combination of fluorescence sensing and imaging allow its' most promising and vibrant method of determination. A ratiometric sensor is highly desirable as it reduces or eliminates the adverse effects of change of environment around the probe (pH, polarity, temperature etc.), probe concentration and excitation power on the emission intensity by providing a built-in correction to the signal ratio of emission intensities at two different wavelengths.³⁻⁵

Zn²⁺ plays pivotal roles in numerous biological processes including brain activity, gene transcription, and immune function etc.⁶ It is employed as a required cofactor that can stimulate the activities of approximately 300 enzymes⁷ including those involved in gene expression and DNA repair.^{8,9} However, abnormal zinc metabolism is associated with many health problems, such as prostate cancer, delayed sexual maturation and impotence, type 2 diabetes mellitus (T2DM), Wilson's diseases, amyotrophic lateral sclerosis (ALS) and age-related macular degeneration (AMD).^{7,10,11} Plausibly, Zn²⁺ homeostasis have some correlation on the pathology of Alzheimer's disease¹² and other severe neurological problems such as cerebral ischemia¹³ and epilepsy.¹⁴

On the other hand, aluminium enters human body through foods and water as Al³⁺, trace amount of which is found in most biological tissues¹⁵ and required for various normal human physiological

processes.¹⁶ However, its excessive exposure (WHO recommended average daily human intake of aluminium is approximately 3–10 mg¹⁷) may cause severe toxicity on human's health, particularly neurotoxicity to damage central nervous system. Disorders of aluminium homeostasis lead to a number of diseases, such as Parkinson's disease (PD), Alzheimer's disease (AD) and amyotrophic lateral sclerosis.¹⁸⁻²¹ In addition, Al³⁺ is suspected to be involved in disease like microcytic hypochromic anemia, myopathy, and affects the absorption of iron in blood causing anemia.^{22,23} Moreover, it inhibits plant growth on acid soils.²⁴

Thus, due to the potential impact of Zn²⁺ and Al³⁺ levels on human health and environment, selective trace level detection of both the ions in a single shot is highly demanding.

Molecular arithmetic to convert chemically encoded information (input) into optical signal as output is the bases of molecular logic gates,²⁵⁻²⁸ a potential scientific interest in the field of unconventional computing systems.²⁹ Examples include AND, OR, XOR, INHIBIT and NAND type molecular level logic gates.³⁰⁻³²

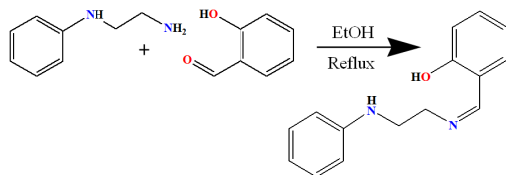
Till date, very few fluorescence sensors³³⁻³⁸ can selectively detect both Zn²⁺ and Al³⁺. Additionally, having similar chemical properties, Cd²⁺ interferes with the Zn²⁺ sensor.³⁹

From practical point of view, a single sensor that shows differential response towards multiple ions is more desirable than one-to-one sensor. These facts stimulated us to search for a single probe that can detect both Zn²⁺ and Al³⁺ selectively.

Recently, our research group has developed a new turn-on Zn²⁺ and Al³⁺ dual sensor⁴⁰. However that is not also the most desirable ratiometric one as already discussed. Ratiometric sensor for dual sensing of Zn²⁺ and Al³⁺ is very rare. A single report from Goswami group⁴¹ have several limitations, viz. the difference between their emission wavelengths is very narrow (14 nm, λ_{em} for Zn²⁺, 446 nm

and λ_{em} for Al^{3+} is 432 nm). Moreover, the ratiometric behaviour is not so prominent/ distinct, while the logic gates constructed are not satisfactory/ useful. Moreover, structures of those probes have not been authenticated by most reliable single crystal X-ray analysis. The same group have recently reported⁴² dual channel detection of Zn^{2+} and Al^{3+} that too has several limitations *viz.* complex and multi-step synthetic protocol with significantly low yield of the probe and used acetonitrile, a very toxic solvent as medium. Moreover, the structure of the Zn^{2+} complex is not authenticated by single crystal X-ray structure analysis.

Addressing those lacunas, we have been able to overcome those limitations and, herein present a molecular probe, L1 capable of dual-sensing Zn^{2+} and Al^{3+} in a ratiometric manner in aqueous-ethanol media with improved detection limits. The sensitivity of L1 towards Zn^{2+} and Al^{3+} is based on inhibition of both ESIPT and CH=N isomerization along with occurrence of CHEF. Additionally, the [L1- Zn^{2+}] complex can selectively detect Al^{3+} under identical experimental conditions. Much lower detection limit with practically no interference have been observed for sensing of Al^{3+} by [L1- Zn^{2+}] complex compared to free organic probe, L1. Furthermore, structures of both L1 and [L1- Zn^{2+}] complex have been confirmed by single crystal X-ray structure analysis. The probe L1 is useful to image both Zn^{2+} and Al^{3+} while the [L1- Zn^{2+}] complex selectively images Al^{3+} in human breast-cancer cells (MCF7) under fluorescence microscope. Experimental findings have been substantiated by theoretical studies too.



Scheme 1

Results and discussion

Spectral studies

Since L1 contains pH sensitive donor sites, its performance is pH sensitive. Emission intensities of L1, both in presence and absence of Zn^{2+} and Al^{3+} are examined at different pH. Fig.S1 and Fig.S2 (ESI) indicate that L1 senses both Zn^{2+} and Al^{3+} over a wide pH range from 6.0 to 11.0. However optimum performance is observed at pH 4.0-8.0. Hence, pH 7.4, being closer to the physiological pH is chosen for the entire studies. All spectral studies have been performed in 0.1 M HEPES buffered aqueous ethanol media (ethanol/water, 1/1, v/v).

The selectivity of L1 towards various common metal ions are examined by addition of 5.0 equiv. Na^+ , K^+ , Ca^{2+} , Mg^{2+} , Cr^{3+} , Mn^{2+} , Fe^{3+} , Co^{2+} , Ni^{2+} , Cu^{2+} , Cd^{2+} , Hg^{2+} , Pb^{2+} , Zn^{2+} and Al^{3+} ions to an aqueous ethanol (1:1, v/v) solution of L1. Fig.1 shows that free L1 displays an emission band at 345 nm (λ_{ex} , 276 nm). Except Zn^{2+} and Al^{3+} , no other common metal ions induce any change to the emission of free L1.

Gradual addition of Zn^{2+} / Al^{3+} (Fig.2/ 3) decreases emission intensity at 345 nm (λ_{ex} , 276 nm) along with the appearance of a new band at 450 nm (blue emission for Zn^{2+}) and 485 nm (green emission for Al^{3+}) which gradually enhances with increasing amount of respective metal ions. The red shift of the emission band is accompanied by 27 fold fluorescence enhancement for Zn^{2+} (λ_{em} , 450 nm, Φ , 0.19, 24 fold enhancement). Similarly 57 fold fluorescence enhancement (λ_{em} , 485 nm, Φ , 0.30, 29 fold enhancement) is observed for Al^{3+} . Moreover, these ratiometric responses are associated with clear isosbestic points at 400 nm for

Zn^{2+} and 415 nm for Al^{3+} . The plots of emission intensity of L1 as a function of added Zn^{2+} and Al^{3+} are presented in Fig.S3 and S4 (ESI) respectively. The linear regions of the plots (Fig.S1a and S2a, ESI) are useful for determination of unknown Zn^{2+} and Al^{3+} concentrations. In presence of Zn^{2+} , 44-fold enhancement of $F_{450/340}$ (0.03277 to 1.43164) has been achieved (Fig.S5, ESI), whereas 100-fold enhancement of $F_{485/340}$ (0.01799 to 1.8112) is observed for Al^{3+} (Fig.S6, ESI). Fluorescence titration profiles provide the association constants of L1 for Zn^{2+} and Al^{3+} as $4.13 \times 10^5 M^{-1}$ and $2.04 \times 10^6 M^{-1}$ following Hill plots⁴³ (Fig.S7 and S8, ESI). The detection limits for Zn^{2+} and Al^{3+} , estimated from fluorescence titration are $2.3 \times 10^{-7} M$ (Fig.S9, ESI) and $2.4 \times 10^{-7} M$ (Fig.S10, ESI) respectively.

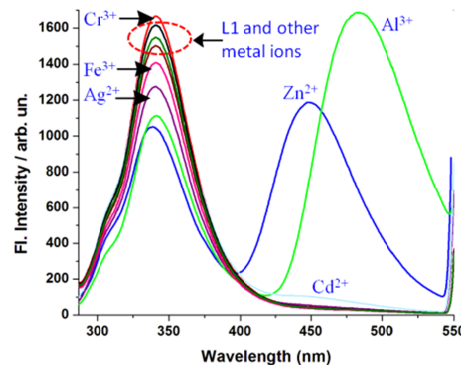


Fig.1 Relative emission intensities of L1 (30 μM) in presence of different metal ions (500 μM) in HEPES buffer (0.1 M, ethanol/ water = 1/1, v/v, pH 7.4) medium, λ_{ex} , 276 nm

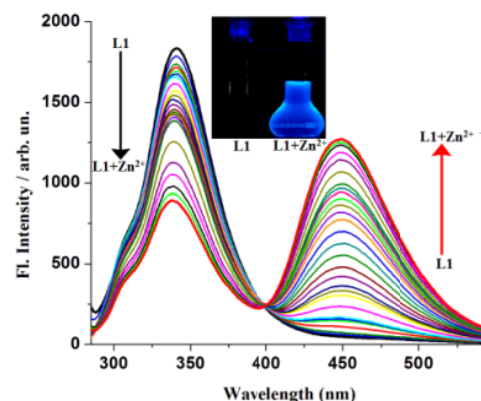


Fig.2 Changes in the fluorescence spectra of L1 (20 μM) in HEPES buffered (0.1 M) solution (ethanol/water = 1:1, v/v, pH 7.4) upon gradual addition of Zn^{2+} (0.5-1000 μM). λ_{ex} = 276 nm, λ_{em} = 340 nm, 450 nm.

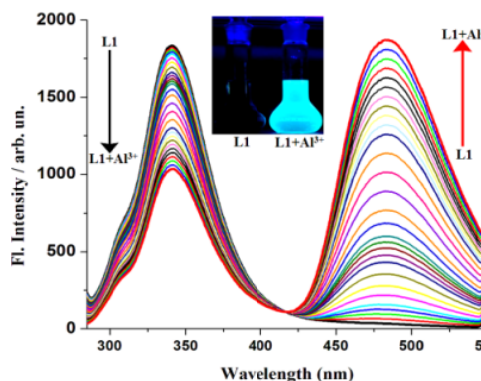


Fig.3 Fluorescence spectral changes of L1 (20 μM) in HEPES buffered (0.1 M) solution (ethanol/water = 1:1 v/v, pH 7.4) upon gradual addition of Al^{3+} (0.5-1000 μM); λ_{ex} = 276 nm, λ_{em} = 340 nm, 485 nm

The chelation of Zn^{2+}/Al^{3+} with O, N donors of L1 increases the rigidity of the molecular assembly by restricting the free rotation around the azomethine functionality and eliminates the ESIP process. These two effects are jointly responsible for the observed fluorescence enhancement (Fig.4).

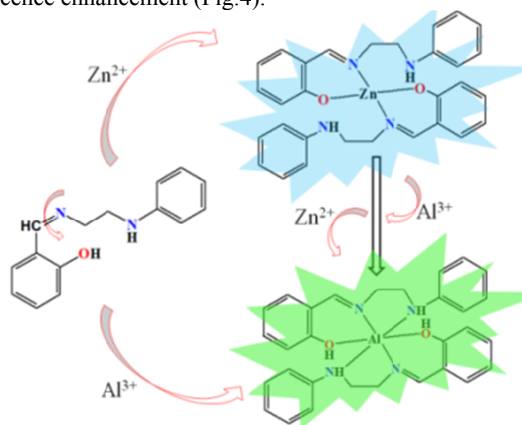


Fig.4 Proposed sensing mechanism of Zn^{2+} and Al^{3+} by L1 and Al^{3+} by $[L1-Zn^{2+}]$ complex

Interestingly, having greater affinity and higher association constant for L1, Al^{3+} easily replaces Zn^{2+} from $[L1-Zn^{2+}]$ complex to form more stable $[L1-Al^{3+}]$ complex. Thus, $[L1-Zn^{2+}]$ complex turns out as a better Al^{3+} sensor and functions *via* displacement approach. Serial addition of Al^{3+} to a solution of the $[L1-Zn^{2+}]$ complex (Fig.5) results red shift of 450 nm emission band (λ_{ex} , 276 nm) to 485 nm along with fluorescence enhancement. This competitive fluorescence titration allows with an improved detection limit for Al^{3+} , 3.3×10^{-8} M (Fig.S11, ESI). Most plausibly, higher co-ordination number of Al^{3+} than Zn^{2+} (> 4) imparts more rigidity to the system (*vide* Fig.4), and minimizes its entropy leading to further fluorescence enhancement.

The effect of competing metal ions on the detection of Zn^{2+}/Al^{3+} is examined to validate the selectivity of L1 for Zn^{2+}/Al^{3+} . Addition of 5.0 equiv. Zn^{2+}/Al^{3+} to L1 in presence of 5.0 equiv. other metal ions shows no significant interferences (Fig.S12 and S13, ESI). Some minor interference for determination of Al^{3+} is completely eliminated employing $[L1-Zn^{2+}]$ complex as Al^{3+} sensor (Fig.S14, ESI). Fig.S15 (ESI) presents the colour changes of L1 upon addition of equimolar various cations under UV light which allows an effective and efficient detection of Zn^{2+} and Al^{3+} .

The absorption spectrum of L1 exhibits a band at 305 nm, attributed to $\pi-\pi^*$ transition. Upon gradual addition of Zn^{2+}/Al^{3+} , the intensity of this band decreases along with the appearance of new bands at 363 nm (for Zn^{2+}), 385 nm (for Al^{3+}). Four well-defined isosbestic points have been observed (Fig.6 and Fig.7). On the other hand, addition of Al^{3+} to $[L1-Zn^{2+}]$ complex reveals that the absorption band initially present at 363 nm decreases with the appearance of a new band at 385 nm (Fig.8). This clearly indicates the displacement of Zn^{2+} from $[L1-Zn^{2+}]$ complex by Al^{3+} to form a thermodynamically favorable $[L1-Al^{3+}]$ complex.

Thus, Zn^{2+} and Al^{3+} dependent shift of emission wavelengths and selective displacement of Zn^{2+} by Al^{3+} from the $[L1-Zn^{2+}]$ complex have allowed us to construct a binary logic gate useful in digital electronics (Fig.9). For input, Zn^{2+}/Al^{3+} defined as "1" state and the absence of any as "0" state. There are two input signals, *viz.* input 1 (Al^{3+}) and input 2 (Zn^{2+}) whereas the output signals correspond to the turn on emission at 485 nm (output 1 due to Al^{3+}) and 450 nm (output 2 due to Zn^{2+}). The logic gates constructed by Goswami group is not at all well-presented, because they have mentioned same output when both Zn^{2+} and Al^{3+} are present together or Al^{3+} present

alone. It will be inconclusive from the output whether Al^{3+} alone or together with Zn^{2+} is present. Our system uses combination of OR and NOT gates along with a switch that describes the situation very clearly. When any of the two inputs (Zn^{2+}/Al^{3+}) is high (three rows in the truth table), the output (at $\lambda_{max} = 450$ nm or 485 nm) is the result of only OR gate (OR1) and the switch is connected to 'A'. When both Zn^{2+} and Al^{3+} inputs are "1" then the output is due to Al^{3+} only, not for Zn^{2+} i.e., at $\lambda_{max} = 485$ nm but not at 450 nm. In this case (last row in the truth table) the switch is connected to 'B'.

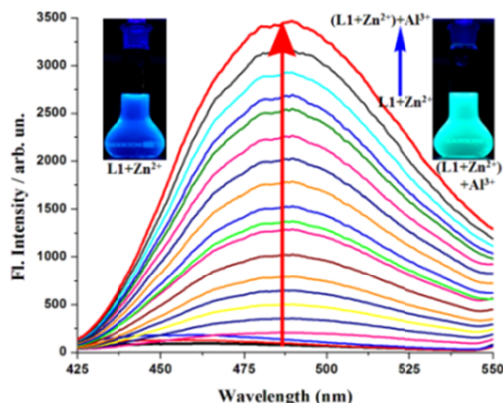


Fig.5 Fluorescence spectral changes of $[L1-Zn^{2+}]$ complex (50 μ M) in HEPES buffered (0.1 M) solution (ethanol/ water = 1:1 v/v, pH 7.4) upon addition of Al^{3+} (0.4-1000 μ M); $\lambda_{ex} = 276$ nm

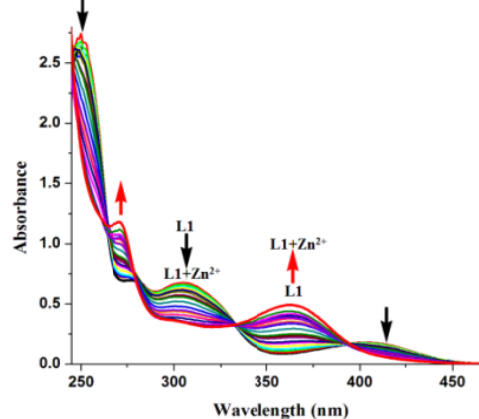


Fig.6 Changes in absorbance of L1 (50 μ M) upon gradual addition of Zn^{2+} (1-3000 μ M) in HEPES buffered (0.1 M) solution (ethanol /water =1:1 v/v, pH 7.4)

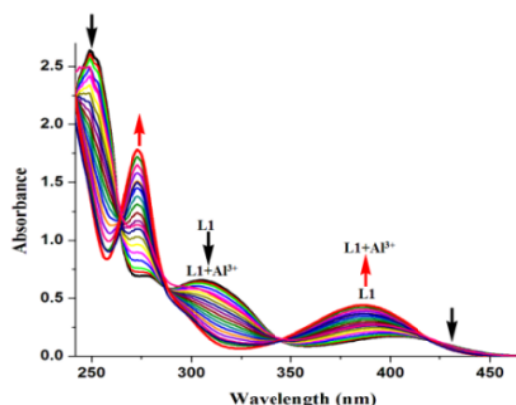


Fig.7 Changes in absorbance of L1 (50 μ M) upon gradual addition of Al^{3+} (1-3000 μ M) in HEPES buffered (0.1 M) solution (ethanol /water =1:1 v/v, pH 7.4)

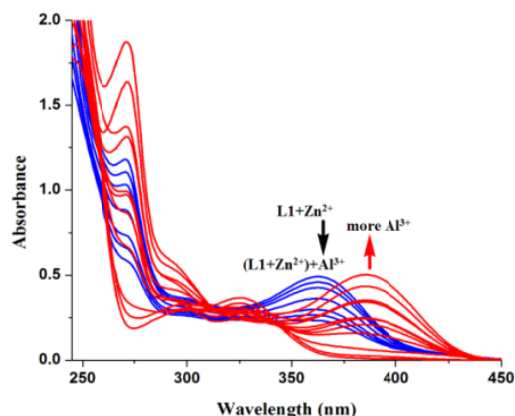


Fig.8 Changes in absorbance of L1 (50 μM) upon gradual addition of Al^{3+} (1–3000 μM) in HEPES buffered (0.1 M) solution (ethanol/water = 1:1 v/v, pH 7.4)

For better understanding of the solution state interaction between L1 with Zn^{2+} and Al^{3+} , ^1H NMR titration experiments have been carried out independently in $\text{CD}_3\text{OD}-\text{D}_2\text{O}$ media (Fig. 10, Fig.S16 and S17, ESI). ^1H NMR spectrum of L1 shows very weak signals of N–H and phenolic O–H protons at 7.53 ppm and 10.06 ppm as expected for their exchangeable character with the solvent protons. Upon addition of 0.5 equiv. Zn^{2+} to L1, the phenolic O–H proton (at 10.06 ppm) disappears (Fig.S16, ESI). Also, the CH=N proton is down-field shifted from 8.35 ppm to 8.37 ppm. On the other hand, upon addition of 0.5 equiv. Al^{3+} , the phenolic O–H protons up-field shifted to some extent from 10.06 to 10.03 ppm with enhanced intensity while the CH=N proton is downfield shifted from 8.35 ppm to 9.27 ppm (Fig.S17, ESI). Moreover, the N–H signal (7.53 ppm for free L1) is downfield shifted to 7.60 ppm with enhanced intensity. These facts suggest the coordination of nitrogen donor sites to Al^{3+} rendering N–H protons non-exchangeable. Other aromatic and aliphatic protons show slight changes for both cases. The results altogether suggest that Al^{3+} is coordinated with the imine nitrogen, hydroxyl oxygen and sp^3 nitrogen donors while Zn^{2+} is coordinated *via* imine nitrogen and hydroxyl oxygen sites of L1. No further change of any proton signals have been observed upon addition of excess metal ions (over 0.5 equiv.) confirming 2:1 complexation between L1 and $\text{Zn}^{2+}/\text{Al}^{3+}$. The same stoichiometry is also supported by the Job's plot (Fig.S18 and S19, ESI). Single crystal X-ray structure of the $[\text{L1}-\text{Zn}^{2+}]$ complex (Fig.S20, ESI) helps to conclude that solid state structure of the complex is retained in solution too. Complexation to Al^{3+} causes relatively higher downfield shifts of the protons of L1, indicating stronger binding relative to Zn^{2+} .

Addition of 5.0 equiv. Al^{3+} to the system containing $[\text{L1} + 5.0$ equiv. $\text{Zn}^{2+}]$ brings the O–H signal back to its position found for $[\text{L1} + 5.0$ equiv. $\text{Al}^{3+}]$ (Fig.10). Further, CH=N proton experiences the desired down-field shift from 8.37 ppm to 9.27 ppm and the N–H signal intensity enhances. The final spectrum looks exactly same to that found after addition of 5.0 equiv. Al^{3+} to L1. All these support stoichiometric displacement of Zn^{2+} from $[\text{L1}-\text{Zn}^{2+}]$ complex by Al^{3+} .

The Zn^{2+} in Fig.S20 adopts a pseudo-tetrahedral coordination, where the tetrahedron is somewhat distorted with $\text{N}(1)-\text{Zn}-\text{O}(3)$ angle being $95.5(3)^\circ$ and $\text{N}(4)-\text{Zn}-\text{O}(1)$ angle being $96.9(4)^\circ$. The $\text{N}(1)-\text{Zn}-\text{N}(4)$ and $\text{O}(1)-\text{Zn}-\text{O}(3)$ angles have opened up to $112.92(12)^\circ$ and $110.78(11)^\circ$ respectively. The Zn–N distance ranging from 1.973(N1) Å to 2.019(N4) Å , while, the Zn–O distance ranging from 1.918(O1) Å to 1.936(O3) Å , are considered normal.⁴⁴ The most significant geometric data are presented in Table

S1 (ESI). The crystal packing of $[\text{ZnL1}]$ complex is shown in Fig.S21 (ESI).

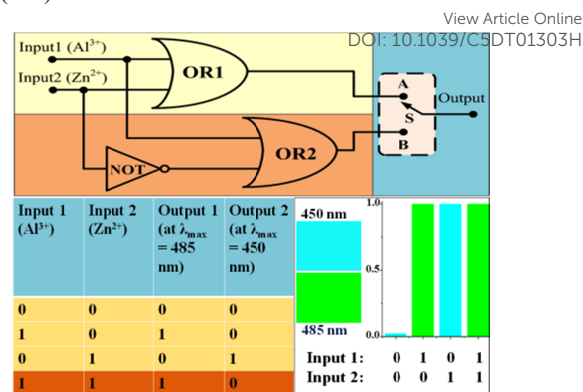


Fig.9 The truth table and logic diagram for simultaneous monitoring of Zn^{2+} and Al^{3+} using L1

Computational studies

Molecular level interactions between L1 and $\text{Zn}^{2+}/\text{Al}^{3+}$ have been studied using density functional theory (DFT) employing B3LYP/6-31G and LanL2dZ basis set.⁴⁵ The HOMO–LUMO energy gaps in free L1, and its $\text{Zn}^{2+}/\text{Al}^{3+}$ adducts are 3.8262 eV, 3.4433 eV and 3.3190 eV respectively (Fig. S22, ESI). With the optimized structures of the complexes, electronic transition energies are calculated by TDDFT method in gas phase and methanol. For methanol, the CPCM formalism is imposed which considers the solvent as a polarisable continuum and do not include discrete solvent molecules for solvation of the solute.⁴⁶ Calculated transition energies for the prominent absorption bands are shown in Table S2 (ESI). Calculated absorption peaks agree well with the experimentally observed peaks. The energy-optimised structure of $[\text{L1}-\text{Zn}^{2+}]$ complex shows distorted octahedral geometry as also found in SC-XRD structure. Thus, very close agreements between the theoretical and experimental findings have been observed.

Cell imaging

L1 is capable to detect intracellular $\text{Zn}^{2+}/\text{Al}^{3+}$ in human breast cancer cells, MCF7 under fluorescence microscope. Cells treated with L1 (without $\text{Zn}^{2+}/\text{Al}^{3+}$) are used as control. Fig.11 indicates that L1 is able to permeate cell membrane to stain $\text{Zn}^{2+}/\text{Al}^{3+}$ without any harm (cells remain alive even after several hours of exposure to 20 μM L1) making it useful to monitor Zn^{2+} or Al^{3+} accumulation in biological systems. Fig.11 also supports the displacement of Zn^{2+} by Al^{3+} from its adduct with L1.

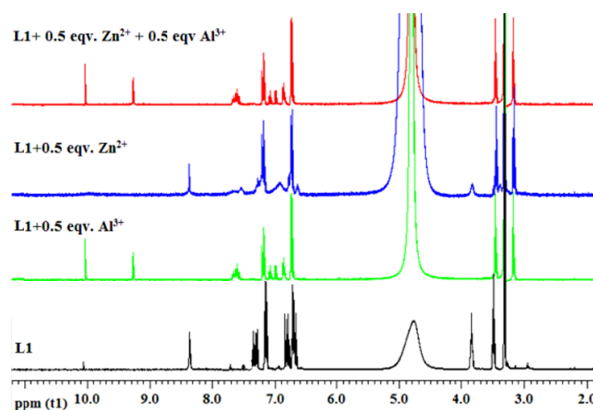


Fig.10 ^1H NMR spectral changes of L1 upon addition of Zn^{2+} and Al^{3+}

Experimental

Apparatus and reagents

High-purity HEPES, salisaldehyde and N-phenyl ethylenediamine are purchased from Sigma Aldrich (India). Zn^{2+} and Al^{3+} stock solutions have been prepared using $Zn(NO_3)_2 \cdot 6H_2O$ and $Al(NO_3)_3 \cdot 9H_2O$ salts respectively. All other metal ions used are either their nitrate or chloride forms. Other analytical reagent grade chemicals are used without further purification except when specified. Water having a resistivity of 18.2 M Ω cm is obtained from a Milli-Q Millipore water purification system (Bedford, MA) and used throughout all the experiments. Solvents used are of spectroscopic grade. A Shimadzu Multi Spec 2450 spectrophotometer is used for recording UV-Vis spectra. FTIR spectra are recorded on a Shimadzu FTIR (model IR Prestige 21 CE) spectrophotometer. Thermo gravimetric analyses are performed on a Perkin Elmer TG/DTA lab system 1 (Technology by SII). Mass spectra have been performed using a QTOF 60 Micro YA 263 mass spectrometer in ES positive mode. 1H and ^{13}C NMR spectrum are recorded using Bruker Avance DPX 300 (300 MHz) in $CDCl_3$. 1H NMR titration experiments have been performed using Bruker Avance DPX 600 (600 MHz) in CD_3OD-D_2O system. Elemental analyses are performed on a Perkin Elmer 2400 CHN analyzer. The steady state emission and excitation spectra are recorded with a Hitachi F-4500 spectrofluorimeter. Systronics digital pH meter (model 335) is used for pH measurement. Fluorescence microscope images are captured through an Olympus IX81 microscope and processed using image-pro plus version 7.0 software.

Synthesis of L1

The probe, L1 has been synthesised by refluxing the equimolar mixture of salisaldehyde and N-phenyl ethylenediamine in ethanol for 6h (Scheme 1). The brown-yellow solid is obtained after evaporation of the solvent. This product is dissolved in methanol and kept at room temperature for slow evaporation. After several days, rectangular yellow crystals suitable for single crystal X-ray diffraction are collected. Yield is 95%. Anal. calcd (%): C, 74.97; H, 6.71 and N, 11.66; found: C, 75.02; H, 6.67 and N, 11.80. The X-ray structure is presented in Fig.S23 (ESI). Significant crystal and refinement parameters are summarized in Table S3 (ESI). 1H NMR (Fig.S24, ESI) (300 MHz, $CDCl_3$), δ (ppm): 3.49 (2H, t, J = 6.0 Hz), 3.79 (2H, t, J = 6.0 Hz), 6.62 (1H, d, J = 0.6 Hz), 6.65 (1H, d, J = 0.9 Hz), 6.72 (1H, t, J = 6.0 Hz), 6.85 (1H, t, J = 6.0 Hz), 6.95 (1H, d, J = 9.0 Hz), 7.16 (1H, d, J = 1.8 Hz), 7.20 (1H, t, J = 1.5 Hz), 7.24 (1H, t, J = 1.8 Hz), 7.29 (1H, t, J = 6.0 Hz), 7.54 (1H, t, J = 1.2 Hz), 8.32 (1H, s), 9.90 (1H, s). ^{13}C NMR (Fig.S25, ESI) (300 MHz, $CDCl_3$), QTOF – MS ES+ (Fig.S26, ESI): $[M + H]^+ = 241.6$. FTIR (cm^{-1}) (Fig.S27, ESI): $\nu(O-H \text{ phenol})$ 3383, $\nu(N-H \text{ } 2^\circ \text{ amine})$ 3360, $\nu(CH=N)$ 1629, $\nu(C-O \text{ phenyl})$ 1315. Thermogram (Fig.S28, ESI) indicates the stability of L1 up to 200°C. UV-Vis. (Fig.S29, ESI): λ (nm) in EtOH (ϵ , $M^{-1} \text{ cm}^{-1}$), 404 nm (8500), 305 nm (32500), 250 nm (132500). Excitation spectrum using emission wavelength is presented in Fig.S29 (ESI).

Synthesis of $[L1+Zn^{2+}]$ complex

Methanol solution of $Zn(NO_3)_2 \cdot 6H_2O$ (50 mg, 0.1680mmol) is added drop-wise to a magnetically stirred solution of L1 (80 mg, 0.3361 mmol) in methanol at room temperature. After 2-3 min, a white precipitate that appeared is filtered and dissolved in minimum volume methylene chloride and kept at room temperature for few days to obtain rectangular white crystals, suitable for X-ray crystallography. Yield is 80%. Anal. calcd (%): C, 66.24; H, 5.56 and N, 10.30; found: C, 66.12; H, 5.49 and N, 10.43. Significant crystal and refinement parameters are summarized in Table S3 (ESI). The QTOF–MS ES⁺ (Fig.S30, ESI) at m/z, 543.30 is assigned to $[2L1^{2-} + Zn^{2+} + H^+]^+$, confirming 2:1 (mole ratio) stoichiometry

between L1 and Zn^{2+} . FTIR (cm^{-1}) (Fig.S31, ESI): $\nu(N-H \text{ } 2^\circ \text{ amine})$ 3294, $\nu(CH=N)$ 1600, $\nu(C-O \text{ phenyl})$ 1303. The absence of $\nu(O-H, \text{ phenol})$ band further confirms deprotonation of L1 upon interaction with Zn^{2+} . Thermogram (Fig.S32, ESI) shows 6.098% weight loss in the temperature range, 40.0-260.7°C corresponds to the loss of two oxygen atoms, and 21.376% weight loss in the temperature range, 260.7-343.3°C, corresponds to the rupture of one CH=N bond along with loss of aldehyde unit. Again, 11.690% weight loss in the temperature range, 343.3-452.9°C corresponds to the breaking of second CH=N bond with loss of corresponding aldehyde unit and 43.530% weight loss in the temperature range, 452.9-566.1°C is attributed to the loss of two amine units. Thermogram also indicates that $[L1+Zn^{2+}]$ complex is more thermally stable (up to 260.7°C) over L1 (up to 200°C). UV-Vis. (Fig.S33, ESI): λ (nm) in EtOH/ H_2O , 1/1, v/v (ϵ , $M^{-1} \text{ cm}^{-1}$): 363 nm (32000), 271 nm (75500). Excitation spectrum using emission wavelength is presented in Fig.S33, (ESI).

Synthesis of $[L1+Al^{3+}]$ complex

A methanol solution of $Al(NO_3)_3 \cdot 9H_2O$ (50 mg, 0.1332 mmol) is added slowly to a magnetically stirred solution of L1 (64 mg, 0.2665 mmol) in methanol. Stirring is continued for 1h. On slow evaporation of the solvent, a deep yellow-brown compound is obtained. Anal. calcd (%): C, 70.99; H, 6.35; N, 11.04; O, 6.30 found: C, 70.82; H, 6.49; N, 10.86; O, 6.17. The compound is characterized by QTOF –MS ES⁺ (Fig.S34, ESI): m/z, 557.1227, attributed to $[2L1 + Al^{3+} + CH_3OH + H_2O]^{3+}$ indicating 2:1 stoichiometry (mole ratio) between L1 and Al^{3+} . FTIR spectrum (Fig.S35, ESI): $\nu(O-H \text{ phenol})$ 3421, $\nu(N-H \text{ } 2^\circ \text{ amine})$ 3251, $\nu(CH=N)$ 1600, $\nu(C-O \text{ phenyl})$ 1303. Thermogram (Fig.S36, ESI) indicates 3.776% weight loss in the temperature range 30.0-60.3°C, attributed to the loss of non-coordinated water molecule. Moreover, 5.527% weight loss in the temperature range, 60.3-90.5°C corresponds to the loss of two OH groups and 42.992% weight loss in the temperature range 90.5-277.9°C is due to the loss of one L1 unit. 14.044% weight loss in the temperature range, 277.9-476.6°C corresponds to the loss of aldehyde unit as a result of rupture of CH=N bond of the remaining L1 moiety. 22.771% weight loss in the temperature range, 476.6-572.1°C is due to the loss of aldehyde part through rupture of CH=N bond of the remaining organic amine part. The presence of non-coordinated water molecule in the $[L1+Al^{3+}]$ complex has also been supported by this thermal analysis. UV-Vis. (Fig.S37, ESI): λ (nm) in EtOH/ H_2O , 1/1, v/v (ϵ , $M^{-1} \text{ cm}^{-1}$): 385 nm (32500), 273 nm (132500). Excitation spectrum using emission wavelength is presented in Fig.S37 (ESI).

The $[L1+Al^{3+}]$ adduct is also prepared by stirring equivalent amount of $Al(NO_3)_3 \cdot 9H_2O$ with the methanol solution of $[L1+Zn^{2+}]$ complex at room temperature. Evaporation of the solvent generates a brown solid having QTOF –MS ES⁺ (Fig.S38, ESI) at m/z, 557.1225, conforming the formation of $[L1+Al^{3+}]$ adduct.

Cell imaging studies

Human breast cancer cell line MCF7 are grown in DMEM (Sigma, St. Louis, USA) supplemented with 10% fetal bovine serum (Sigma, St. Louis, USA), 2 mM glutamine, 100 U/ mL penicillin-streptomycin solution (Gibco, Invitrogen, USA) in presence of 5% CO_2 at 37°C. For *in vitro* imaging studies, the cells are seeded in 6 well culture plate with a seeding density of 10^5 cells per well. After reaching 60%–70% confluence, the previous media is replaced with serum free media, supplemented Zn^{2+} , Al^{3+} and L1 at a concentration of 50, 50 and 20 μM , and incubated for 2h to facilitate their uptake by cells. The cells are then observed under an inverted microscope at different magnifications to examine any adverse effect on cellular morphology. L1 treated cells are then incubated with Zn^{2+} and Al^{3+} alone for 15 – 30 min or with Zn^{2+} followed by Al^{3+} and observed

under fluorescence microscope. Control experiment is performed using the said medium devoid of any metal salts.

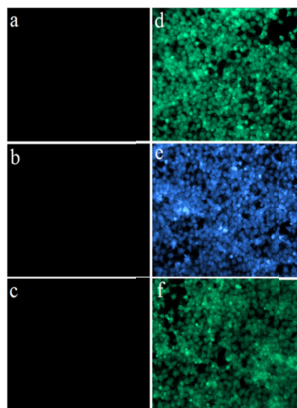


Fig.11 Fluorescence image of the MCF7 cells after incubation for 2h with (a) L1 (20 μ M), (b) Al^{3+} (50 μ M), and (c) Zn^{2+} (50 μ M), (d) 20 μ M L1 followed by addition of 50 μ M Al^{3+} , (e) 20 μ M L1 followed by addition of 50 μ M Zn^{2+} , (f) 20 μ M L1+ 50 μ M Zn^{2+} followed by addition of 50 μ M Al^{3+}

Conclusions

In summary, L1 is an efficient ratiometric sensor for Zn^{2+} that can detect Al^{3+} as well and function through ESIP and CHEF mechanism. Moreover, [L1- Zn^{2+}] complex has higher sensitivity for Al^{3+} functioning via displacement approach. Both the structures for L1 and [L1- Zn^{2+}] complex have been authenticated by single crystal X-ray analysis. The sensing of Zn^{2+} and Al^{3+} has been digitalized through construction of a binary logic gate (combination of OR and NOT gates) that function as a molecular switch. The excellent sensing process has been materialized in fluorescence cell imaging studies.

Acknowledgements

We are grateful to UGC-DAE-KC for funding and CAS (UGC) for infrastructural facilities. We are grateful to Dr. Arnab Banerjee, University of Texas, Austin for cell imaging studies. We sincerely acknowledge Dr. S. Karmakar, USIC, BU for help regarding XRD analysis.

Notes and references

- 1 A. Chatterjee, M. Santra, N. Won, S. Kim, J.K. Kim, S.B. Kim and K.H. Ahn, *J. Am. Chem. Soc.*, 2009, **131**, 2040.
- 2 Y. Ni and J. Wu; *Org. Biomol. Chem.*, 2014, **12**, 3774.
- 3 W.T. Mason in *Fluorescent and Luminescent Probes for Biological Activity*, 2nd. Ed. (Ed.: W.T. Mason), Academic Press, London 1999, pp. 175.
- 4 Y. Kawanishi, K. Kikuchi, H. Takakusa, S. Mizukami, Y. Urano, T. Higuchi and T. Nagano, *Angew. Chem. Int. Ed.*, 2000, **39**(19), 3438.
- 5 J. Fan, M. Hu, P. Zhan and X. Peng, *Chem. Soc. Rev.*, 2013, **42**, 29.
- 6 (a) C. J. Frederickson, J.Y. Koh and A.I. Bush, *Nat. Rev. Neurosci.*, 2005, **6**, 449; (b) E.L. Que, D.W. Domaille and C.J. Chang, *Chem. Rev.*, 2008, **108**, 1517.
- 7 Z. Dai and J.W. Canary, *New J. Chem.*, 2007, **31**, 1708–1718
- 8 T.V. O'Halloran, *Science*, 1993, **261**, 715.
- 9 E. Ho, B.N. Ames, *Proc. Natl. Acad. Sci. U.S.A.*, 2002, **99**, 16770.
- 10 K. Jobe, C.H. Brennan, M. Motevalli, S.M. Goldup and M. Watkinson, *Chem. Commun.*, 2011, **47**, 6036.

- 11 H. Sharma, N. Singh and D.O. Jang, *Tetrahedron Letters*, 2014, **55**(49), 6623.
- 12 M. P. Cuajungco and G. J. Lees, *Neurobiol. Dis.*, 1997, **4**, 137.
- 13 J. Y. Koh, S. W. Suh, B. J. Gwag, Y. Y. He, C. Y. Hsu and D. W. Choi, *Science*, 1996, **272** (5264), 1013.
- 14 C. J. Frederickson, M. D. Hernandez and J. F. McGinty, *Brain Res.*, 1989, **480**, 317.
- 15 (a). H. M. Park, B. N. Oh, J. H. Kim, W. Qiong, K. D. Jung and C. Kim, *Tetrahedron Lett.*, 2011, **52**, 5581; (b). D. R. Burwen, S. M. Olsen, L. A. Bland, M. J. Arduino, M. H. Reid and W. R. Jarvis, *Kidney Int.*, 1995, **48**, 469; (c). G. Berthon, *Coord. Chem. Rev.*, 2002, **228**, 319.
- 16 G. H. Robinson, *Chem. Eng. News*, 2003, **81** (36), 54.
- 17 (a). J. Barcelo and C. Poschenrieder, *Environ. Exp. Bot.*, 2002, **48**, 75; (b). Z. Krejpcio and R.W. Wojciak, *Pol. J. Environ. Stud.*, 2002, **11**, 251.
- 18 E. Altschuler, *Med. Hypotheses*, 1999, **53**, 22.
- 19 B. Wang, W. Xing, Y. Zhao and X. Deng, *Environ. Toxicol. Pharmacol.*, 2010, **29**, 308.
- 20 J. R. Walton, *Neurotoxicology*, 2006, **27**, 385.
- 21 S. Polizzi, *Neurotoxicology*, 2002, **23**, 761–774.
- 22 A. Dhara, A. Jana, N. Guchhait, P. Ghosh and S.K. Kar, *New J. Chem.*, 2014, **38**, 1627.
- 23 A. Sahana, A. Banerjee, S. Das, S. Lohar, D. Karak, B. Sarkar, S. K. Mukhopadhyay, A. K. Mukherjee and D. Das, *Org. Biomol. Chem.*, 2011, **9**, 5523.
- 24 E. Delhaize and P. R. Ryan, *Plant Physiol.*, 1995, **107**, 315.
- 25 K. Szacilowski, *Chem. Rev.*, 2008, **108**, 348.
- 26 S. Ozlem and E.U. Akkaya, *J. Am. Chem. Soc.*, 2009, **131**, 48
- 27 U. Pischel, *Angew. Chem., Int. Ed.*, 2007, **46**, 4026.
- 28 A. P. de Silva and N. D. McClenaghan, *Chem. Eur. J.*, 2004, **10**, 574.
- 29 V. Balzani and F. Scandola, *Supramolecular Photochemistry*, Ellis-Horwood: Chichester, 1991.
- 30 A. P. de Silva, H. Q. N. Gunaratne and G. E. M. Maguire, *J. Chem. Soc., Chem. Commun.*, 1994, 1213.
- 31 A. Credi, V. Balzani, S.J. Langford and J.F. Stoddart, *J. Am. Chem. Soc.*, 1997, **119**, 2679.
- 32 A. Banerjee, A. Sahana, S. Das, S. Lohar, B. Sarkar, S.K. Mukhopadhyay, J.S. Matalobos and D. Das, *Dalton Trans.*, 2013, **42**, 16387.
- 33 P. Du and S. J. Lippard, *Inorg. Chem.*, 2010, **49**, 10753.
- 34 K. Soroka, R.S. Vithanage, D.A. Phillips, B. Walker and P. K. Dasgupta, *Anal. Chem.*, 1987, **59**, 629.
- 35 D. Maity and T. Govindaraju, *Chem. Commun.*, 2012, **48**, 1039.
- 36 M. Shellaiah, Y.H. Wu, H.C. Lin, *Analyst*, 2013, **138**, 2931.
- 37 W.H. Ding, W. Cao, X.J. Zheng, W.J. Ding, J.P. Qiao and L.P. Jin, *Dalton Trans.*, 2014, **43**, 6429.
- 38 W. Cao, X. J. Zheng, J.P. Sun, W.T. Wong, D.C. Fang, J.X. Zhang and L.P. Jin, *Inorg. Chem.*, 2014, **53**, 3012.
- 39 X. Liu, N. Zhang, J. Zhou, T. Chang, C. Fang and D. Shangguan, *Analyst*, 2013, **138**, 901.
- 40 S. Lohar, A. Sengupta, A. Chattopadhyay, J.S. Matalobos and D. Das, *Eur. J. Inorg. Chem.*, 2014(33), 5675.
- 41 S. Goswami, S. Paul and A. Manna, *RSC Adv.*, 2013, **3**, 25079.
- 42 S. Goswami, A. Manna, S. Paul, A.K. Maity, P. Saha, C.K. Quah and H.K. Fun, *RSC Adv.*, 2014, **4**, 34572.
- 43 (a). H. Y. Lin, P. Y. Cheng, C. F. Wan and A. T. Wu, *Analyst*, 2012, **137**, 4415; (b). W. H. Hsieh, C. F. Wan, D. J. Liao and A. T. Wu, *Tetrahedron Lett.*, 2012, **53**, 5848.
- 44 (a). M. Amirasr, A. H. Mahmoudkhani, A. Gorji, S. Dehghanpour and H.R. Bijanzadeh, *Polyhedron*, 2002, **21**, 2733; (b). H.K. Liu, W.Y. Sun, D.J. Ma, K.B. Yub and W.X. Tang, *Chem. Commun.*, 2000, 591.

- 45 Gaussian 03, Rev.C.02 (Gaussian Inc., Wallingford CT), 2004.
- 46 (a). S. Miertus, E. Scrocco and J. Tomasi, *Chem. Phys.*, 1981, **55**, 117; (b). M. Cossi, V. Barone, R. Cammi and J. Tomasi, *Chem. Phys. Lett.*, 1996, **255**, 327; (c). M. Cossi, V. Barone and M. A. J. Robb, *Chem. Phys.*, 1999, **111**, 5295; (d). M. Cossi, G. Scalmani, N. Rega and V. J. Barone, *Chem. Phys.*, 2002, **117**, 43.

View Article Online
DOI: 10.1039/C5DT01303H

Dalton Transactions Accepted Manuscript